Article

Label-Free Tracking of Proteins through Plasmon-Enhanced Interference

Matthew Peters, Declan McIntosh, Alexandra Branzan Albu, Cuifeng Ying, and Reuven Gordon*

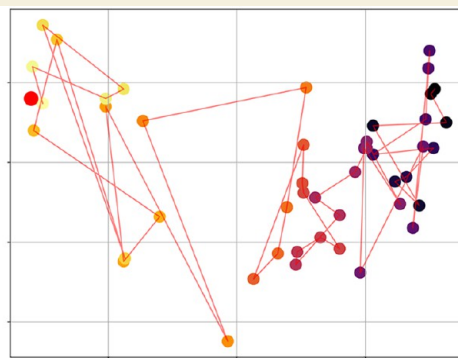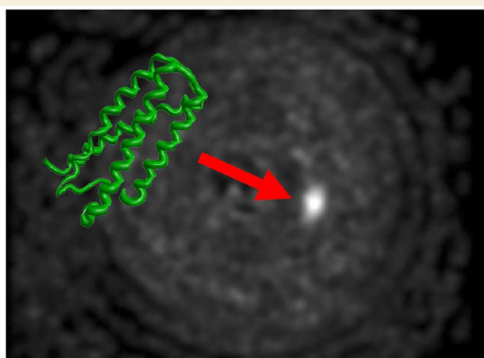Cite This: *ACS Nanosci. Au* 2024, 4, 69−75

Read Online

ACCESS | Metrics & More | Article Recommendations | Supporting Information

ABSTRACT: Single unmodified biomolecules in solution can be observed and characterized by interferometric imaging approaches; however, Rayleigh scattering limits this to larger proteins (typically >30 kDa). We observe real-time image tracking of unmodified proteins down to 14 kDa using interference imaging enhanced by surface plasmons launched at an aperture in a metal film. The larger proteins show slower diffusion, quantified by tracking. When the diffusing protein is finally trapped by the nanoaperture, we perform complementary power spectral density and noise amplitude analysis, which gives information about the protein. This approach allows for rapid protein characterization with minimal sample preparation and opens the door to characterizing protein interactions in real time.

KEYWORDS: single molecule imaging, plasmonics, protein tracking, label-free biosensing, tether-free biosensing, nanoaperture optical tweezers

INTRODUCTION

The dominant approaches to observing single proteins and their dynamics and interactions involve modifying the protein with fluorescent labels and/or tethers.[1] These modifications often alter the protein's biophysical properties and limit the observation time due to quenching.[2−4] When investigating unknown targets, labeling can be challenging since interactions are not predefined. For example, new methods of kinetic screening of antibodies developed from hybridoma technologies aid monoclonal antibody development.[5] Thus, it is desirable to seek out methods that can directly observe single unmodified proteins to complement fluorescent measurements. This remains challenging since particles much smaller than the wavelength of light have scattering that diminishes with the sixth power of the radius.[6]

Several techniques have emerged to quantify single proteins without labels. Interferometric scattering (iSCAT) has imaged single proteins in solution without modifications.[7−10] Due to inherent contrast limitations, iSCAT has been limited to 40 kDa detection, but machine learning and lengthy frame averaging has pushed detection to 9 kDa, albeit with only 60% precision.[11] Additionally, the tracking of proteins has not been performed without the addition of strong scatterers such as gold nanoparticles to amplify the movement.[12−15]

Plasmonic scattering microscopy (PSM) has been shown to image nonspecific single protein binding using interference from surface plasmon resonance sensors and analytes.[16] The evanescent field only extends ≃100 nm away from the surface so bulk impurities in solution do not affect the imaged results and images the transmitted signal to avoid the strong reflection from the gold surface. Currently, this has been shown to image the binding of a 35 kDa protein in solution, but it is unable to track its diffusion.[17−19]
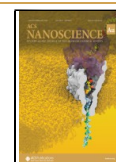
Nanofluidic scattering microscopy (NSM) utilizes subwavelength channels combined with dark-field microscopy to track the diffusion of single proteins through interference with the
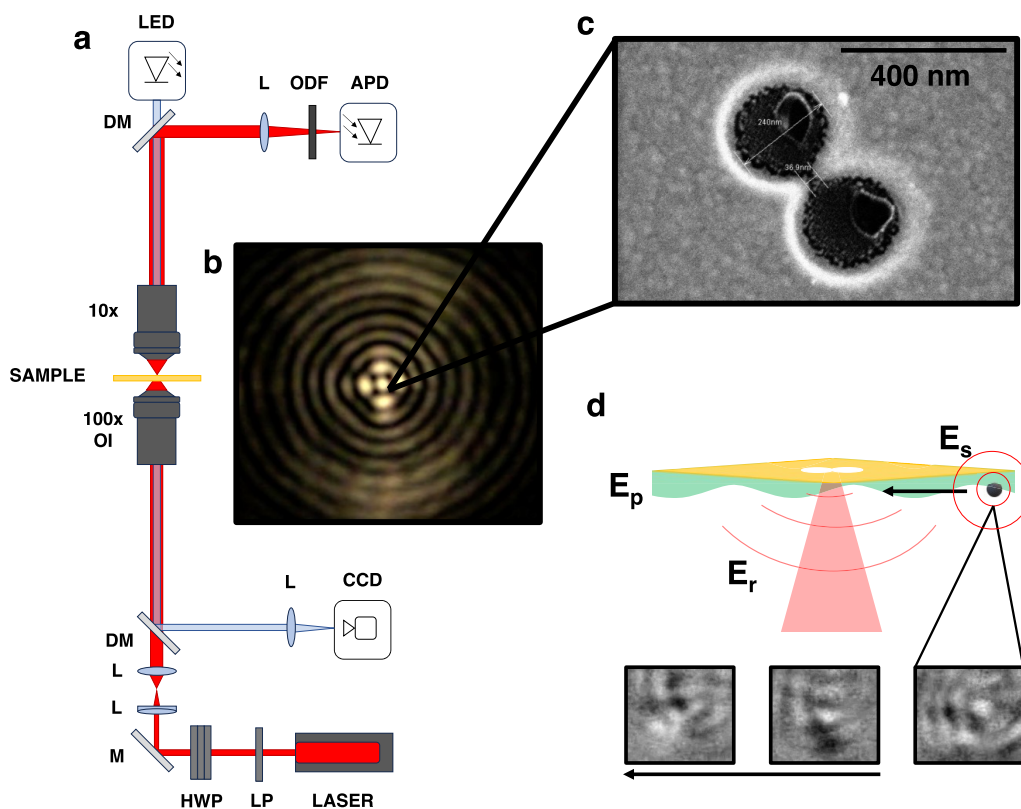
Figure 1. Experimental setup showing the (a) optical tweezers and (b) camera image of the reflected laser fringe pattern. LED: light-emitting diode. APD: avalanche photodiode. ODF: optical density filter. L: lens. DM: dichroic mirror. OI: oil immersion. CCD: charge-coupled device. M: mirror. HWP: half-waveplate. LP: linear polarizer. (c) Scanning electron microscope image of a double nanohole. (d) Illustration of PEPTI with interference pattern changes as the protein moves toward the center. Scattering from the protein (E_s) interferes with the surface plasmon wave (E_p) and the reflected laser (E_r).
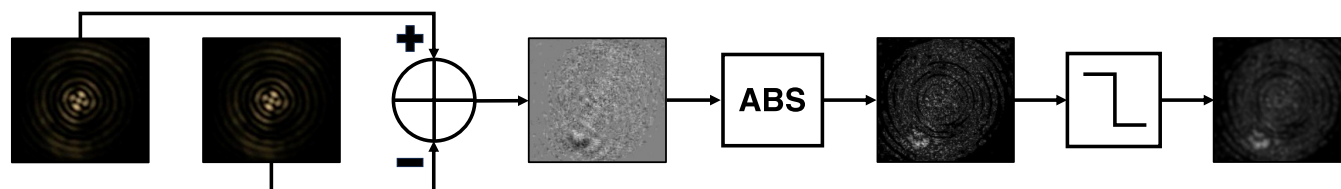
Figure 2. Block diagram of image processing. First, the two sequential images are subtracted. ABS indicates that the absolute value is taken, followed by a Gaussian and median filter indicated by a low-pass filter symbol.

channel. This method is able to size single proteins using the optical contrast of a differential image and demonstrates tracking down to 66 kDa.[20]

These methods rely on an interference between the particle scattering and a reference signal, and the signal scales with the volume of the particle. Even with high laser powers and long averaging, these techniques are typically not able to observe proteins below 30 kDa, which accounts for half the human proteome.[21]

By combining the surface plasmon interference with the reflected laser beam interference, we observe light scattering to track the diffusion of single unmodified proteins in real time adjacent to a nanoaperture in a gold film. We track proteins as small as 14 kDa with a copious signal (so smaller proteins will be resolvable in the future). We observe that diffusion is faster for smaller proteins, as expected from their reduced Stokes' drag. The observed signal has fringes showing interference scattering but also contains a surface plasmon contribution due to the adjacent gold surface; therefore, we believe the

extraordinary sensitivity achieved combines the physical principles that have enabled iSCAT and PSM so far. We observe the trajectory of various proteins as they approach the nanoaperture and are trapped. Once trapped, further analysis on the protein is performed using nanoaperture tweezer techniques, as previously established.[22]

UNMODIFIED SINGLE PROTEIN TRACKING

Figure 1a shows the experimental setup used for tracking proteins. A modified optical tweezer was used, with a double nanohole (DNH) in a gold film placed in the path of the laser. Figure 1b shows the interference pattern produced by the laser focused on a DNH (Figure 1c), which allows for the observation of a particle moving in the vicinity of the DNH. A schematic of the experimental approach we call plasmon-enhanced protein tracking with interference (PEPTI) is shown in Figure 1d. Surface plasmon waves are launched by focusing an 850 nm laser on a nanostructure in gold. The surface plasmon waves interfere with the scattering of the protein.
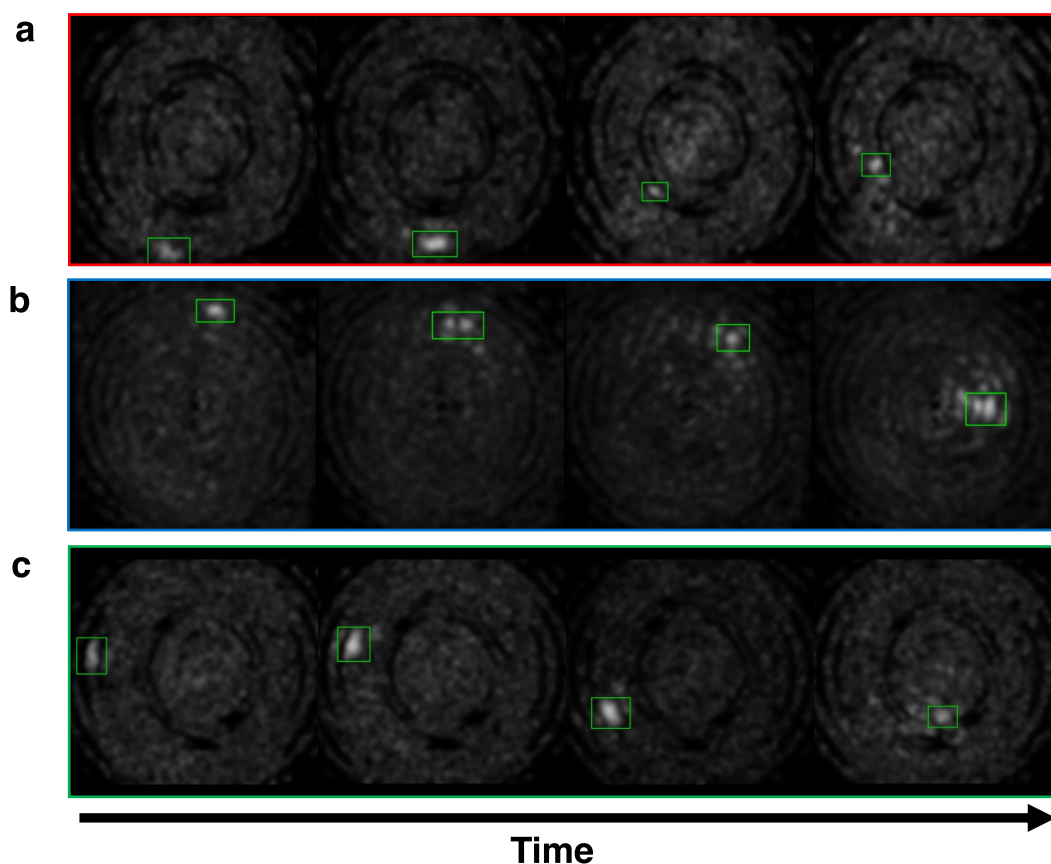
Figure 3. Representative detection events for proteins over time: (a) bovine serum albumin, (b) carbonic anhydrase, and (c) cytochrome C.
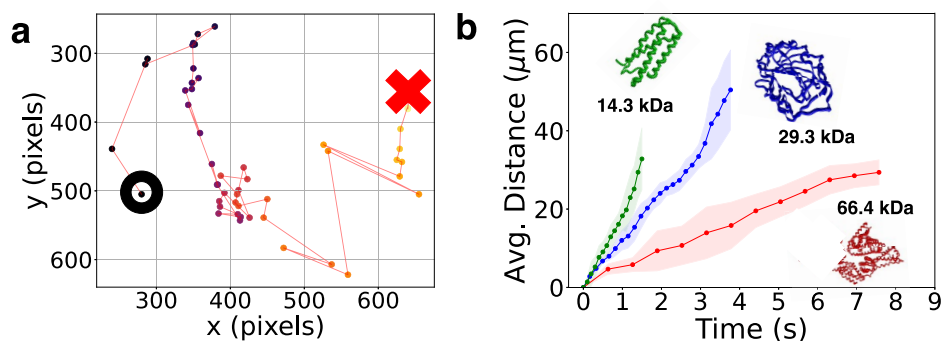

Figure 4. (a) Tracking of a single cytochrome C protein. The black circle represents the start of tracking and the red X represents the trapping point. (b) Average cumulative distances traveled with standard deviations for each protein. Total events were 4 BSA, 5 CA, and 6 CTC.

Direct observation of protein scattering is masked by laser reflections; however, the fringes act as a semiconstant medium that is perturbed by the enhanced plasmon−protein scattering. The phase difference between the surface plasmons and protein scattering give rise to a strong interference term, and an additional interference effect is present from the gold reflection and protein scattering that further enhances the signal.

While the overall scattering (E_s), including interference from the aperture scattering (E_p) with the direct reflection from the gold film (E_r), shows dynamic variation, the ability to track the protein arises by differential analysis, as seen in Figure 2. The single frame subtraction is computationally efficient, allowing for real-time tracking without the need for frame averaging. The previous frame was subtracted from the current frame, giving rise to an image with negative and positive components.

The interference effect was verified using a common reference for background removal; this showed a similar result to differential subtraction, indicating that the plus/minus signal is due to phase differences and not due to movement of the protein between frames. The absolute value of the differential image was taken and then smoothed with a Gaussian filter ($\sigma = 8$) and a median filter to reduce the noise. A Roboflow 3.0 object detection model was trained on 19 672 frames from 15 videos and contained augmented images as well. This algorithm was used to detect the protein and track the position. The detection and tracking algorithms run with linear order, enabling scalable quasi-real-time detection.

Detection for three standard globular proteins of different sizes is shown in Figures 3a−3c. The contrast of the protein image does not follow the usual third power scaling for interference effects: for proteins with molecular weights of
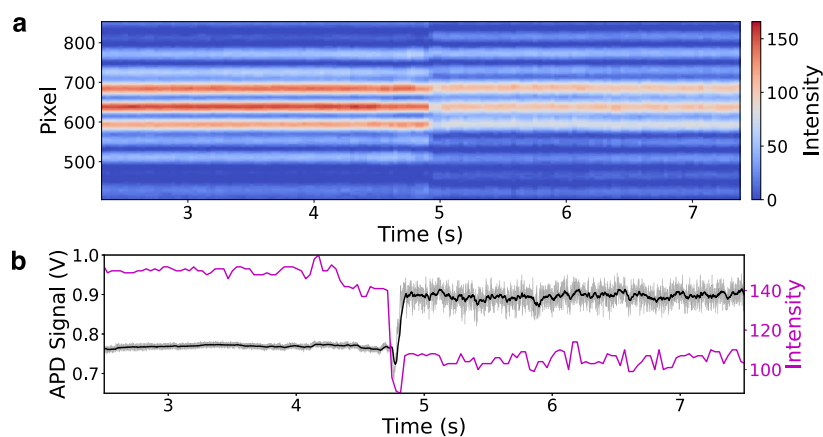
Figure 5. (a) Time evolution of a row of pixels through the center of the frame; trapping is distinctly shown as a decrease in signal. (b) Correlation of a single pixel from the center band tracked over time with the APD signal measuring the transmission.

14.3, 29.3, and 66.4 kDa, the maximum pixel intensities are 141 ± 19, 127 ± 17, and 137 ± 28, respectively, as shown in Figure S7. The scattering intensity is related to the distance from the surface: the evanescent nature of the surface plasmon contribution means that the smaller proteins are able to get closer to the surface (on the order of nanometers) and the interaction is stronger. PSM does not see this same scaling because they image proteins binding to antibodies at a fixed distance from the surface, not making full use of the evanescent field directly adjacent to the surface. The SNR of PEPTI is remarkable compared with iSCAT; a typical iSCAT for a 40 kDa protein has an SNR of 3.[11] We show the detection and tracking of a 14.3 kDa protein with an SNR of 3.5, with only a single frame subtraction. Since the contrast has not shown scaling with the volume of the protein, the lower limit of detection should be much smaller. Due to the complex nature of the bright spot obtained, sizing the protein through a 2D Gaussian fit is not possible. Instead, it is possible to size the protein through the speed at which it diffuses.

The diffusion speed can be obtained by measuring the cumulative distance that the protein travels over time. Tracking of a single cytochrome C protein is shown in Figure 4a. The average cumulative distances traveled for proteins bovine serum albumin (BSA, 66.4 kDa), carbonic anhydrase (CA, 29.3 kDa), and cytochrome C (CTC, 14.3 kDa) are shown in Figure 4b. The diffusion seems to follow the molecular weight with the distance traveled: CTC, CA, and BSA traveled 29.2, 18.5, and 7.9 μm in 1.5 s, respectively, showing the expected trend that smaller proteins diffuse faster. As the protein moves closer to the trapping point, the diffusion becomes constrained by the trapping volume and forces present in the area. The diffusion near the trap is packed, as seen in some trajectories of Figures S4−S6. Overall, the diffusion is slower than expected from unconstrained 3D diffusion.

COMPLEMENTARY NANOAPERTURE OPTICAL TWEEZER ANALYSIS

We have shown that it is possible to track single protein diffusion in solution until it is trapped, giving us the ability to perform further analysis on the same protein. Nanoaperture optical trapping (NOT) is already a well-established technique for single protein measurements.[22−28] Taking a row slice through the fringe pattern shown in Figure 1b, the video (found in the Supporting Information) can be treated as a one-dimensional signal akin to the APD transmission measurement,

as shown in Figure 5a. The fringes in the video are shown as distinct bands in the waveform, with the highest intensity correlating to the center lobe. Information complementary to the APD signal is observed in Figure 5b when comparing a single pixel from the center band over time to the APD signal. Despite the opposite collection modes and substantially different sampling rates, the video (reflection) and APD (transmission) are able to characterize trapping distinctly as a change in signal level at the same time, showing that we are measuring the same protein we observed diffusing. The camera pixel intensity shows a decrease in the reflection during trapping, as expected by the increased transmission from dielectric loading. To verify that we are seeing single proteins, a NOT analysis was performed and is shown in Figures S1d and S1e. The time constant and normalized root mean squared deviation of the trapped proteins both follow the expected trends for sizing single proteins in previously established methods.[29]

DISCUSSION

The plasmonic scattering from the DNH is polarization-sensitive, and it was found qualitatively that aligning the laser polarization to excite both polarization components of the aperture (i.e., between the extrema in transmission) gave a suitable trade-off between image quality and trapping ability. Finite-difference-time-domain simulations were performed and show that the reflection depends on polarization, as seen in the Figure S2. The imaging area is governed by the reflected laser signal seen in the camera as the perturbations in the fringes are used to highlight the protein. The number of fringes and the size of the pattern is dictated by the focus of the laser on the gold. Imaging was performed successfully in a range of areas from 280−580 μm². When trapping proteins, maximum transmission through the aperture is desired, and this results from being under-focused on the aperture. A larger imaging area can be achieved by being further under-focused at the expense of trapping performance. A signal with significantly larger contrast and brightness is seen when compared to PSM and iSCAT, so that neither plasmonic interference nor reflection interference scattering play the sole role in PEPTI. In fact, a combination of effects must be present: the surface plasmon scattering interference as described by the PSM must work in conjunction with scattering from the protein due to the incident laser beam and the laser reflected off of the gold to provide an exceptionally strong signal. While past works on

PSM have shown a departure from sixth power to third power scaling in experiments due to surface plasmons,[16] here the scattering contrast for the 14 and 66 kDa proteins is approximately the same. We do not believe that we can predict the observed size dependence with electromagnetic simulations alone. The benefit of PEPTI is the minimal processing required, and single frame removal enables real-time imaging of single proteins. Other algorithms were tested, including frame averaging combined with differential removal and a Gaussian mixture model, but none of them proved to be superior for tracking. While not analyzed here, the videos contain information after trapping related to the protein position inside the nanoaperture and the stiffness of the trap.

The videos used for tracking (see the Supporting Information) have a frame rate of 30 frames per second, much less than the APD sampling rate and many high performance cameras. This is not a fundamental limit, and future studies should be able to make use of high-speed cameras with frame rates approaching a million frames per second even; especially since we use filters to attenuate the laser signal to avoid saturation and reduce the camera gain and so there is a copious signal for faster imaging. This is especially interesting for observing fast folding and conformational dynamics while not requiring tethering and for studying interactions with proteins, DNA, RNA, antibodies, or other biomolecules.

CONCLUSION

We have demonstrated the detection and tracking of single proteins in solution down to 14 kDa with copious signals to push detection limits even further. This technique does not require fluorescent labels nor does it require binding to a substrate. Compared with similar methods (iSCAT, PSM, and NSM), our approach is able to significantly detect smaller proteins, with the caveat that iSCAT has used machine learning to detect small proteins, albeit with only 60% precision. We observe size-dependent diffusion with the smallest proteins diffusing fastest, as expected based on drag, and can combine this technique with optical trapping to perform complementary analysis on the protein. Future directions could aim to look at protein interactions and high-speed dynamics.

METHODS

Sample Fabrication

A 75 × 50 × 1 mm glass microscope slide (Fisherbrand) was cut into three pieces using a diamond scribe, the dust was removed by rinsing with ethanol, and the pieces were blow-dried with nitrogen. These pieces were then sonicated in ethanol for 10 min, rinsed with ethanol and acetone, and blow-dried again with nitrogen gas. A final visual inspection was performed to ensure that there are no large pieces of dust remaining on the slide and that there were no scratches. Polystyrene spheres (PS) were used to form the mask, and 10 μL of the 300 nm PS (Sigma-Aldrich MFCD00131491 LB3) and 1 mL of ethanol were mixed gently. Following the mixing, 7.5 μL of the diluted PS solution was deposited in a zigzag pattern using a micropipette. The coated slides were left overnight for the ethanol to evaporate while the PS formed dimers at random. After evaporation, the coated slides were treated with a plasma cleaner for 170 s using a Harrick PDC plasma cleaner to shrink the polystyrene and thereby control the dimer cusp size.

Titanium (7 nm), followed by gold (70 nm), was sputtered onto the coated slides using a Mantis QUBE system. Double-sided polyamide tape was used to adhere the samples to the mounting plate with the coated side facing outward. The samples were removed from the Mantis system and then sonicated for 2 min in a beaker with ethanol. The samples were placed in the beaker so they leaned against the side to ensure that the PS fell off and the gold was not scratched. The samples were rinsed with ethanol and blow-dried with nitrogen. The gold samples were cut into quarters using a diamond scribe and blow-dried to remove dust. The samples were then plasma-cleaned for 10 min and immediately placed in a jar of ultrapure water.

Solution Preparation

Prior to preparing any solution, a 60 × 24 × (0.16−0.19) mm coverslip (Fisherbrand 22-266-882P) was rinsed with isopropyl alcohol, acetone, and ethanol. The coverslip was blow-dried with nitrogen gas and placed on lens paper. An image spacer (Grace Bio-Laboratories GBL-654008-100EA) was attached to the coverslip, and 9.5 μL of the solution was pipetted into the spacer. The gold DNH sample was placed on top of the spacer so the gold was in contact with the solution.

Proteins

The proteins used in the experiments came from a Sigma-Aldrich size-standard kit (MWGF70-1KT). Bovine serum albumin, carbonic anhydrase, and cytochrome C were prepared with a concentration of $0.1 \frac{wt}{v}\%$. The proteins were weighed in 1.5 mL Eppendorf tubes and then dissolved in a 0.01 M phosphate-buffered saline solution.

Data Acquisition

An Advantech USB-4711A data acquisition unit (100 kS/s, 12-bit) collected the APD signal. Advantech DAQ Data Logger Express was used to display the live data. The data were analyzed in both MATLAB and Python.

Data Analysis

All analysis of APD data was performed in Python. All measurements were performed on distinct samples. The sample sizes were 5 for BSA, 9 for CA, and 7 for CTC. A low-pass filter with a cutoff frequency of 10 Hz was used when plotting the avalanche photodiode signal.

Power Spectral Density. The power spectral density was calculated using a 5 s portion of the trapped data. The absolute value squared was taken and then Fourier-transformed. The positive spectrum was used and fit to a Lorentzian function of the form $\frac{A}{f^2 + f_c^2}$, where f_c is the corner frequency. The autocorrelation function measures the similarity between a signal and its time-delayed version, whereas the power spectral density function gives the distribution of average power in the frequency domain. Since the autocorrelation shows an exponential dependence and the PSD is the Fourier transform of autocorrelation, the corner frequency is the inverse of the time constant.[30]

Time Constant. The time constant is related to the corner frequency obtained from the power spectral density by $\frac{1}{2\pi f_c}$.

Normalized RMSD. The trapped signal was divided into sections based on the length of the signal divided by window length (5000). The RMSD was calculated for each section as $\sqrt{\frac{1}{n} \sum_{i=1}^{n} (\hat{x}_i - x_i)^2}$ and then divided by the mean of the trapped signal, and the average of all of these sections was taken. This was repeated for the laser signal before trapping. The laser RMSD was then subtracted from the trapped RMSD.

Image Processing

Videos were recorded with a ThorLabs DCU224C-BG camera (1280 × 1024 pixels, 1.31 megapixel) and uc480 software from ThorLabs. A minimum exposure time and gain were used as allowed by the camera; RGB channel gains were equal. The object detection algorithm contained 9998 frames from the videos and a total of 19 672 images obtained from augmenting the data set. The training set contained 14 661 images (75%), the validation set contained 2935 images (15%), and the test set contained 2076 images (10%). A manual check for all videos was performed to ensure accuracy.

Distance traveled statistics were performed with four BSA videos, five CA videos, and six CTC videos. All videos were distinct samples.

Distance Calculations. An x,y coordinate was obtained from the detected protein in the video. The interpoint distance was calculated from $\sqrt{(x_2 - x_1)^2 + (y_2 - y_1)^2}$.

■ ASSOCIATED CONTENT

Ⓢ Supporting Information

The Supporting Information is available free of charge at https://pubs.acs.org/doi/10.1021/acsnanoscienceau.3c00045.

Movies of raw and processed protein tracking (ZIP) Nanoaperture optical trapping analysis; finite-difference-time-domain simulations of nanoapertures; finite-difference-time-domain simulations of field enhancement for three polarizations; all tracking data for CTC, CA, and BSA; protein contrast values; distances traveled; and the protein properties (PDF)

■ AUTHOR INFORMATION

Corresponding Author

Reuven Gordon − *Department of Electrical Engineering, University of Victoria, Victoria, British Columbia V8W 2Y2, Canada; Centre for Advanced Materials & Related Technologies (CAMTEC), University of Victoria, Victoria, British Columbia V8W 2Y2, Canada;* ⓘ orcid.org/0000-0002-1485-6067; Email: rgordon@uvic.ca

Authors

Matthew Peters − *Department of Electrical Engineering, University of Victoria, Victoria, British Columbia V8W 2Y2, Canada; Centre for Advanced Materials & Related Technologies (CAMTEC), University of Victoria, Victoria, British Columbia V8W 2Y2, Canada;* ⓘ orcid.org/0000-0001-8835-7917

Declan McIntosh − *Department of Electrical Engineering, University of Victoria, Victoria, British Columbia V8W 2Y2, Canada*

Alexandra Branzan Albu − *Department of Electrical Engineering, University of Victoria, Victoria, British Columbia V8W 2Y2, Canada*

Cuifeng Ying − *Advanced Optics and Photonics Laboratory, Department of Engineering, School of Science & Technology, Nottingham Trent University, Nottingham NG11 8NS, U.K.;* ⓘ orcid.org/0000-0002-7279-1388

Complete contact information is available at:
https://pubs.acs.org/10.1021/acsnanoscienceau.3c00045

Notes

The authors declare no competing financial interest.

■ ACKNOWLEDGMENTS

■ REFERENCES

(1) Kubitscheck, U. *Fluorescence microscopy: from principles to biological applications*; John Wiley & Sons: NJ, 2017.

(2) Quinn, M.; Gnan, N.; James, S.; Ninarello, A.; Sciortino, F.; Zaccarelli, E.; McManus, J. How fluorescent labelling alters the solution behaviour of proteins. *Phys. Chem. Chem. Phys.* **2015**, *17*, 31177−31187.

(3) Gajraj, A.; Ofoli, R. Y. Effect of extrinsic fluorescent labels on diffusion and adsorption kinetics of proteins at the liquid- liquid interface. *Langmuir* **2000**, *16*, 8085−8094.

(4) Bingaman, S.; Huxley, V. H.; Rumbaut, R. E. Fluorescent dyes modify properties of proteins used in microvascular research. *Microcirculation* **2003**, *10*, 221−231.

(5) Kim, M.; Foster, J. C.; Moore, M. D.; Chen, M. Improving single-molecule antibody detection selectivity through optimization of peptide epitope presentation in OmpG nanopore. *ACS Sensors* **2023**, *8*, 2673−2680.

(6) Booth, L. S.; Browne, E. V.; Mauranyapin, N. P.; Madsen, L. S.; Barfoot, S.; Mark, A.; Bowen, W. P. Modelling of the dynamic polarizability of macromolecules for single-molecule optical biosensing. *Sci. Rep.* **2022**, *12*, 1995.

(7) Ortega-Arroyo, J.; Kukura, P. Interferometric scattering microscopy (iSCAT): new frontiers in ultrafast and ultrasensitive optical microscopy. *Phys. Chem. Chem. Phys.* **2012**, *14*, 15625−15636.

(8) Ortega Arroyo, J.; Andrecka, J.; Spillane, K.; Billington, N.; Takagi, Y.; Sellers, J.; Kukura, P. Label-free, all-optical detection, imaging, and tracking of a single protein. *Nano Lett.* **2014**, *14*, 2065−2070.

(9) Foley, E. D.; Kushwah, M. S.; Young, G.; Kukura, P. Mass photometry enables label-free tracking and mass measurement of single proteins on lipid bilayers. *Nat. Methods* **2021**, *18*, 1247−1252.

(10) Cole, D.; Young, G.; Weigel, A.; Sebesta, A.; Kukura, P. Label-free single-molecule imaging with numerical-aperture-shaped interferometric scattering microscopy. *ACS Photonics* **2017**, *4*, 211−216.

(11) Dahmardeh, M.; Mirzaalian Dastjerdi, H.; Mazal, H.; Köstler, H.; Sandoghdar, V. Self-supervised machine learning pushes the sensitivity limit in label-free detection of single proteins below 10 kDa. *Nat. Methods* **2023**, *20*, 442−447.

(12) McDonald, M. P.; Gemeinhardt, A.; König, K.; Piliarik, M.; Schaffer, S.; Völkl, S.; Aigner, M.; Mackensen, A.; Sandoghdar, V. Visualizing single-cell secretion dynamics with single-protein sensitivity. *Nano Lett.* **2018**, *18*, 513−519.

(13) Liebel, M.; Hugall, J. T.; Van Hulst, N. F. Ultrasensitive label-free nanosensing and high-speed tracking of single proteins. *Nano Lett.* **2017**, *17*, 1277−1281.

(14) Kukura, P.; Ewers, H.; Müller, C.; Renn, A.; Helenius, A.; Sandoghdar, V. High-speed nanoscopic tracking of the position and orientation of a single virus. *Nat. Methods* **2009**, *6*, 923−927.

(15) Taylor, R. W.; Mahmoodabadi, R. G.; Rauschenberger, V.; Giessl, A.; Schambony, A.; Sandoghdar, V. Interferometric scattering microscopy reveals microsecond nanoscopic protein motion on a live cell membrane. *Nat. Photonics* **2019**, *13*, 480−487.

(16) Zhang, P.; Ma, G.; Dong, W.; Wan, Z.; Wang, S.; Tao, N. Plasmonic scattering imaging of single proteins and binding kinetics. *Nat. Methods* **2020**, *17*, 1010−1017.

(17) Zhang, P.; Wang, R.; Wan, Z.; Zhou, X.; Ma, G.; Kolay, J.; Jiang, J.; Wang, S. Label-Free Imaging of Single Proteins and Binding Kinetics Using Total Internal Reflection-Based Evanescent Scattering Microscopy. *Anal. Chem.* **2022**, *94*, 10781−10787.

(18) Zhang, P.; Ma, G.; Wan, Z.; Wang, S. Quantification of single-molecule protein binding kinetics in complex media with prism-coupled plasmonic scattering imaging. *ACS Sensors* **2021**, *6*, 1357−1366.

(19) Zhang, P.; Zhou, L.; Wang, R.; Zhou, X.; Jiang, J.; Wan, Z.; Wang, S. Evanescent scattering imaging of single protein binding kinetics and DNA conformation changes. *Nat. Commun.* **2022**, *13*, 2298.

(20) Spackova, B.; Klein Moberg, H.; Fritzsche, J.; Tenghamn, J.; Sjosten, G.; Sipova-Jungova, H.; Albinsson, D.; Lubart, Q.; van Leeuwen, D.; Westerlund, F.; Midtvedt, D.; Esbjorner, E. K.; Kall, M.; Volpe, G.; Langhammer, C. Label-free nanofluidic scattering microscopy of size and mass of single diffusing molecules and nanoparticles. *Nat. Methods* **2022**, *19*, 751−758.

(21) Li, Z.-l.; Buck, M. Beyond history and "on a roll": The list of the most well-studied human protein structures and overall trends in the protein data bank. *Protein Sci.* **2021**, *30*, 745−760.

(22) Gordon, R. Biosensing with nanoaperture optical tweezers. *Optics & Laser Technology* **2019**, *109*, 328−335.

(23) Pang, Y.; Gordon, R. Optical trapping of a single protein. *Nano Lett.* **2012**, *12*, 402−406.

(24) Neumeier, L.; Quidant, R.; Chang, D. E. Self-induced back-action optical trapping in nanophotonic systems. *New J. Phys.* **2015**, *17*, 123008.

(25) Peri, S. S. S.; Sabnani, M. K.; Raza, M. U.; Ghaffari, S.; Gimlin, S.; Wawro, D. D.; Lee, J. S.; Kim, M. J.; Weidanz, J.; Alexandrakis, G. Detection of specific antibody-ligand interactions with a self-induced back-action actuated nanopore electrophoresis sensor. *Nanotechnology* **2020**, *31*, 085502.

(26) Hong, C.; Yang, S.; Ndukaife, J. C. Stand-off trapping and manipulation of sub-10 nm objects and biomolecules using opto-thermo-electrohydrodynamic tweezers. *Nat. Nanotechnol.* **2020**, *15*, 908−913.

(27) Verschueren, D.; Shi, X.; Dekker, C. Nano-optical tweezing of single proteins in plasmonic nanopores. *Small Methods* **2019**, *3*, 1800465.

(28) Yousefi, A.; Ying, C.; Parmenter, C. D. J.; Assadipapari, M.; Sanderson, G.; Zheng, Z.; Xu, L.; Zargarbashi, S.; Hickman, G. J.; Cousins, R. B.; Mellor, C. J.; Mayer, M.; Rahmani, M. Optical monitoring of in situ iron loading into single, native ferritin proteins. *Nano Lett.* **2023**, *23*, 3251−3258.

(29) Wheaton, S.; Gordon, R. Molecular weight characterization of single globular proteins using optical nanotweezers. *Analyst* **2015**, *140*, 4799−4803.

(30) Chaparro, L.; Akan, A. *Signals and Systems using MATLAB*; Academic Press, 2018.